Atmos. Meas. Tech. Discuss., 7, 7569–7611, 2014
www.atmos-meas-tech-discuss.net/7/7569/2014/
doi:10.5194/amtd-7-7569-2014

Atmospheric Measurement Techniques Discussions

SPARTAN: a global network to evaluate and enhance satellite-based estimates of ground-level particulate matter for global health applications

G. Snider[1], C. L. Weagle[2], R. V. Martin[1,2,3], A. van Donkelaar[1], K. Conrad[1], D. Cunningham[1], C. Gordon[1], M. Zwicker[1], C. Akoshile[4], P. Artaxo[5], N. X. Anh[6], J. Brook[7], J. Dong[8], R. M. Garland[9], R. Greenwald[10], D. Griffith[11], K. He[8], B. N. Holben[12], R. Kahn[12], I. Koren[13], N. Lagrosas[14], P. Lestari[15], Z. Ma[10], J. Vanderlei Martins[16], E. J. Quel[17], Y. Rudich[13], A. Salam[18], S. N. Tripathi[19], C. Yu[10], Q. Zhang[8], Y. Zhang[8], M. Brauer[20], A. Cohen[21], M. D. Gibson[22], and Y. Liu[10]

[1]Department of Physics and Atmospheric Science, Dalhousie University, Halifax, Canada
[2]Department of Chemistry, Dalhousie University, Halifax, Canada
[3]Harvard-Smithsonian Center for Astrophysics, Cambridge, MA 02138, USA
[4]Department of Physics, University of Ilorin, Ilorin, Nigeria
[5]Instituto de Física, Universidade de São Paulo, Rua do Matão, Travessa R, 187, São Paulo, SP 05508-090, Brazil

[6]Institute of Geophysics, Vietnam Academy of Science and Technology, Hanoi, Vietnam
[7]Department of Public Health Sciences, University of Toronto, Toronto, Ontario, M5S 1A8, Canada
[8]Center for Earth System Science, Tsinghua University, Beijing, China
[9]Unit for Environmental Science and Management, North West University, Potchefstroom, South Africa
[10]Rollins School of Public Health, Emory University, 1518 Clifton Road NE, Atlanta, GA 30322, USA
[11]Council for Scientific and Industrial Research (CSIR), Pretoria, South Africa
[12]Earth Science Division, NASA Goddard Space Flight Center, Greenbelt, Maryland, USA
[13]Department of Earth and Planetary Sciences, Weizmann Institute, Rehovot 76100, Israel
[14]Manila Observatory, Ateneo de Manila University campus, Quezon City, Philippines
[15]Faculty of Civil and Environmental Engineering, Institute of Technology Bandung (ITB), JL. Ganesha No. 10, Bandung 40132, Indonesia
[16]Department of Physics and Joint Center for Earth Systems Technology, University of Maryland, Baltimore County, Baltimore, Maryland, USA
[17]UNIDEF (CITEDEF-CONICET) Juan B. de la Salle 4397 – B1603ALO Villa Martelli, Buenos Aires, Argentina
[18]Department of Chemistry, University of Dhaka, Dhaka – 1000, Bangladesh
[19]Center for Environmental Science and Engineering, Indian Institute of Technology, Kanpur, India
[20]School of Population and Public Health, University of British Columbia, Vancouver, British Columbia, Canada
[21]Health Effects Institute, 101 Federal Street Suite 500, Boston, MA 02110-1817, USA
[22]Department of Process Engineering and Applied Science, Dalhousie University, Halifax, Nova Scotia, Canada

Received: 24 June 2014 – Accepted: 30 June 2014 – Published: 23 July 2014

Correspondence to: G. Snider (graydon.snider@dal.ca)

Published by Copernicus Publications on behalf of the European Geosciences Union.

Abstract

Ground-based observations have insufficient spatial coverage to assess long-term human exposure to fine particulate matter ($PM_{2.5}$) at the global scale. Satellite remote sensing offers a promising approach to provide information on both short- and long-term exposure to $PM_{2.5}$ at local-to-global scales, but there are limitations and outstanding questions about the accuracy and precision with which ground-level aerosol mass concentrations can be inferred from satellite remote sensing alone. A key source of uncertainty is the global distribution of the relationship between annual average $PM_{2.5}$ and discontinuous satellite observations of columnar aerosol optical depth (AOD). We have initiated a global network of ground-level monitoring stations designed to evaluate and enhance satellite remote sensing estimates for application in health effects research and risk assessment. This Surface PARTiculate mAtter Network (SPARTAN) includes a global federation of ground-level monitors of hourly $PM_{2.5}$ situated primarily in highly populated regions and collocated with existing ground-based sun photometers that measure AOD. The instruments, a three-wavelength nephelometer and impaction filter sampler for both $PM_{2.5}$ and PM_{10}, are highly autonomous. Hourly $PM_{2.5}$ concentrations are inferred from the combination of weighed filters and nephelometer data. Data from existing networks were used to develop and evaluate network sampling characteristics. SPARTAN filters are analyzed for mass, black carbon, water-soluble ions, and metals. These measurements provide, in a variety of global regions, the key data required to evaluate and enhance satellite-based $PM_{2.5}$ estimates used for assessing the health effects of aerosols. Mean $PM_{2.5}$ concentrations across sites vary by an order of magnitude. Initial measurements indicate that the AOD column to $PM_{2.5}$ ratio is driven temporally primarily by the vertical profile of aerosol scattering; and spatially by a more complex interaction of the aerosol scattering vertical profile and by the mass scattering efficiency.

1 Introduction, motivation, and problem definition

$PM_{2.5}$ (particulate matter with a median aerodynamic diameter less than 2.5 µm) is a robust indicator of mortality and other adverse health effects associated with ambient air pollution (Chen et al., 2008; Laden et al., 2006). Research on long-term exposure to ambient $PM_{2.5}$ has documented serious adverse health effects, including increased mortality from chronic cardiovascular disease, respiratory disease, and lung cancer (WHO, 2005). The Global Burden of Disease 2010 estimated that outdoor $PM_{2.5}$ caused 3.2 ± 0.4 million deaths (3.0 % of all deaths) and 76 (+9.0, −8.1) million years of lost healthy life on a global scale in the year 2010 (Lim et al., 2012). Given the implications and uncertainties of this estimate, additional attention is needed to improve global estimates of $PM_{2.5}$ exposure.

Routine measurements of long-term average concentrations of $PM_{2.5}$ have until very recently been generally limited to North America and Europe. Research on adverse $PM_{2.5}$ health effects can only be conducted where information exists about population exposures. As a result, the epidemiologic evidence of chronic exposure to fine particles comes primarily from studies conducted in low-$PM_{2.5}$ locations. Elsewhere in the world, in regions thought to have the highest ground-level concentrations of $PM_{2.5}$ (including large parts of Asia, Africa, and the Middle East) there is little or no long-term surface monitoring of $PM_{2.5}$ (Brauer et al., 2011; Friedl et al., 2010). Research on the health effects of long-term $PM_{2.5}$ exposure in these regions has been limited (HEI, 2010). Risk assessments such as the Global Burden of Disease (Lim et al., 2012) have had to rely on uncertain extrapolation of North American and European epidemiologic study results. Despite recent increases in $PM_{2.5}$ surface monitoring in some locations such as in parts of Asia, ground-level measurements of $PM_{2.5}$ are still far too sparse in terms of spatial and temporal coverage to be used in long-term exposure estimates, or to supplement satellite remote-sensing. Aerosol concentration estimates from chemical transport models are uncertain in highly populated areas (Anenberg et al., 2010; Fang et al., 2013; Punger and West, 2013). Existing PM_{10} measurements (e.g. Brauer et al.,

2011) and airport observations of visibility (Husar et al., 2000) can only partially address the needs of global-scale health impact assessment. Global publicly available $PM_{2.5}$ data are needed in multiple urban centres and highly populated rural zones, for epidemiologic research and health-based risk assessments.

Satellite remote sensing of ground-level particulate matter, when combined with external constraints of aerosol vertical profiles from chemical transport models, has emerged as a promising solution to this need. This hybridized detection method is being increasingly applied in epidemiologic research and risk assessment (e.g. Crouse et al., 2012). However remote sensing continues to require additional validation and analysis to support its widespread use for health-related applications on a global scale. There are outstanding questions about the accuracy and precision with which ground-level long-term $PM_{2.5}$ mass concentrations can be inferred from discontinuous AOD observations (Hoff and Christopher, 2009; Paciorek and Liu, 2009). Factors that affect the relation of satellite AOD observations to long-term $PM_{2.5}$ include the aerosol vertical profile, the conversion of ambient extinction to dry $PM_{2.5}$ mass, $PM_{2.5}$ diurnal variation, and cloud-free sampling biases. Measurements of ground-level $PM_{2.5}$ collocated with AOD measurements are needed to evaluate model calculations of $PM_{2.5}$ / AOD ratios and, in turn, improve estimates of surface $PM_{2.5}$ from satellite AOD retrievals. Composition information is also needed, as a variety of studies link $PM_{2.5}$ composition to health outcomes (e.g. Bell et al., 2011; Lippmann, 2014) and for its ability to inform the mass extinction coefficient. Particulate matter composition is also useful for source attribution (Kong et al., 2010) and for understanding aerosol formation processes (e.g. Hand et al., 2012).

Accurate AOD is measured from a network of ground-based sun photometers. The Aerosol Robotic Network (AERONET) is a remarkably successful federation of sun photometer stations that provides global, long-term, continuous, and publicly available data, in particular of AOD (Holben et al., 1998). AERONET is extensively used for satellite validation and provides temporally resolved measurements during daylight hours at

0.01 to 0.02 mid-visible AOD accuracy. Other sun photometer networks provide additional measurement locations (e.g. Kahn et al., 2004).

In this paper we describe the development and measurement approaches of the Surface PARTiculate mAtter Network (SPARTAN), which is specifically designed to evaluate and enhance satellite-based estimates of ground-level particulate matter and to reduce uncertainties in their use for global health applications. SPARTAN collects both midday aerosol measurements needed to compare with satellite overpass times and the 24 h $PM_{2.5}$ averages relevant for health studies. This document provides an overview of steps toward the development of SPARTAN. Section 2 describes the site selection process and prioritization. Section 3 provides a general overview of SPARTAN instrumentation. Section 4 introduces some initial results.

2 SPARTAN site selection and prioritization

The overarching purpose of SPARTAN is to evaluate and enhance satellite remote sensing estimates of ground-level $PM_{2.5}$ in populated areas. Given this objective, we used several criteria to identify priority SPARTAN sites: (i) high population density is desirable for relevance to global public health. (ii) Collocation with existing sun photometers provides high quality measurements of AOD currently used for satellite evaluation. (iii) Locations should span a wide range of $PM_{2.5}$ concentrations and composition. (iv) Locations are preferred where satellite-based $PM_{2.5}$ estimates have higher uncertainty or where little publicly available $PM_{2.5}$ data exists. (v) Locations should represent spatial scales of typical satellite products of > 3 km $\times$ 3 km (Appendix A1 assesses the spatial representativeness of single measurement sites compared with satellite observation area). (vi) Safety of personnel and equipment is also considered.

Figure 1 shows current and potential sites spanning regions with low (e.g. Manila and Halifax) to high (e.g. Beijing and Kanpur) $PM_{2.5}$. Locations include regions impacted by biomass burning (e.g. West Africa, South Asia), biofuel use (e.g. South Asia), monsoonal conditions (e.g. West Africa, Southeast Asia) and mineral dust (e.g. West Africa,

Middle East). Exact site placement depends on specific partnerships and the availability of resources and personnel. Table 1 lists confirmed host sites to date. The sires of Halifax, Atlanta and Mammoth Cave are included for instrument intercomparison purposes.

3 SPARTAN instrumentation

3.1 General overview

SPARTAN is composed of ground-based instruments that measure fine particle concentrations and allow for the determination of some compositional features (i.e. black carbon, major metals and water-soluble ions). Our primary focus is on determining $PM_{2.5}$ mass. We subdivide this goal into estimating hourly, 24 h mean, and long-term (annual and seasonal) concentrations. Daily mean $PM_{2.5}$ is related to AOD (total column) measurements during daytime satellite overpass times. Coarse aerosol mass, defined as $PM_c \equiv PM_{10} - PM_{2.5}$, is measured in order to assess PM_{10} concentrations. Coarse mass provides additional information on the particle size distribution of relevance for both aerosol optical properties and health effects. A major consideration for the instrumentation is capability for near-autonomous operation. Cost-efficiencies are considered given the grass-roots nature of this work.

Each SPARTAN site includes a combination of continuous monitoring by nephelometry and mass concentration from sampling on filters. Nephelometer backscatter and total light scatter at three wavelengths provides high temporal resolution and some information on particle size. We calibrate nephelometer light scattering with filter-based measurements over multi-day intervals, hence the combination of these measurements yields hourly $PM_{2.5}$ values.

All SPARTAN instruments to date have been designed and manufactured by AirPhoton, LLC (www.airphoton.com). Attributes of these instruments include low maintenance, portability, and field readiness. Installation is straightforward; both the

nephelometer and air sampler mount directly to a secure support pole. Sections 3.2 and 3.3 summarize the most recent instrument designs but will likely be modified as the network matures. Total power consumption is minimal (34 W) and the instruments have been successfully operated in Nigeria using a solar panel and battery. Martins et al. (2014) will provide more detail about the instrument characteristics and performance.

3.2 Impaction measurements: concept and strategy

Filter-based measurements are collected using an AirPhoton SS4i automated air sampler. Each station houses a removable filter cartridge inside a weather-resistant Pelican case such that the filter inlet faces downwards. Airflow and backpressure are logged every 15 s onto a memory card with capacity for two or more years of data. The 8 slot filter cartridge protects the filters during transport to the field and reduces the frequency of site visits. Sampled cartridges are then mailed to the central SPARTAN cleanroom laboratory at Dalhousie University every two months.

Figure 2 shows a diagram of the filter assembly. Each cartridge contains 7 pairs of preweighed 25 mm diameter, 2 µm pore size PTFE (225-2726, SKC) and capillary membrane (custom grease-coated E8025-MB, SPI) filters sampled actively at 4 L min^{-1} for the programmed period. An eighth cartridge slot contains a travelling blank. An important aspect of this filter assembly design is the automatic switching between filter pairs. Incoming aerosols pass through a bug screen and a greased (ultra-high vacuum) impactor plate, which traps aerosols larger than 10 µm in diameter. Coarse-mode (PM_c) particles are then removed by a capillary (Nuclepore) membrane (8 µm pore diameter, 5 % porosity). The concept of employing capillary filters for size selection has been well-established (Heidam, 1981; John et al., 1983; Parker et al., 1977). This stacked filter unit (SFU) arrangement has similarities with the Gent model (Hopke et al., 1997) and the SFU design has been shown to compare well with other aerosol filter systems (Hitzenberger et al., 2004). The 50 % aerosol capture efficiency is at approximately 2.5 µm for the selected flow rate and pore size (Chow, 1995; John et al.,

1983). Coarse-mode solid particles may, however, be susceptible to particle bounce; to prevent their lower capture efficiency the capillary pore surfaces are coated with a thin layer of vacuum grease by the manufacturer (SPI) (John et al., 1983). Fine mode ($PM_{2.5}$) aerosols are collected on 2 µm fibre PTFE filters surfaces, which are compatible with a variety of chemical analyses (Chow, 1995).

3.2.1 Intermittent air filter sampling procedure

The SPARTAN sampling procedure is designed to cost-effectively measure long-term $PM_{2.5}$ concentrations. Each filter pair collects for 160 min each day over a period of nine days for a total of 24 h of sampling per filter. Nine-day periods have been chosen to avoid day-of-week biases. Similar duty-cycle sampling protocols have been used in other spatial air monitoring campaigns (Larson et al., 2007). When sampling stops after the 9 day period, the instrument switches to a new filter slot and the next sampling period begins. With seven active filter slots each cartridge can therefore operate unattended in the field for a 63 day interval. We tested the behaviour of semivolatile material (ammonium nitrate) in the cartridge to diurnal heating cycles. Based on our experiments a moderate loss rate of ammonium nitrate can be expected from the PTFE filters while warm air actively flows over the filters (cf. Appendix A2) but these loss rates are minimal during periods when there is no active sampling. We choose to start and end sampling runs for each filter in the morning (09:00 LT) when temperatures are lower to increase retention of semivolatile material. For example, the first day of sampling will be from 09:00–11:40 LT while the last period runs from 06:20 to 09:00 LT. Appendix A3 describes tests, using USA EPA data for hourly-reported $PM_{2.5}$, where we find that representativeness errors for annual mean concentrations inferred from staggered sampling as used here are substantially reduced compared with the traditional 1-in-*N* day sampling for the same total sample time. Capillary and PTFE filters have a maximum particle loading before a loss of flow is apparent. For locations with higher particulate matter concentrations we reduce the sampling time between 15 % and 100 % within each 2 h 40 min period to prevent clogging, as described in Appendix A4. During the

staggered air samplings the collocated nephelometer measures particle light scattering continuously.

3.2.2 Filter analysis

All filters are analyzed at Dalhousie University for mass, black carbon, water-soluble ions, and metals. These measurements provide the key data required for modelling the $PM_{2.5}$ / AOD ratio and for assessing the health effects of aerosols. After air sampling is complete and filter cartridges are returned to Dalhousie University, post-analysis begins with gravimetric filter weighing. Capillary membrane and PTFE filters are equilibrated for 24 h before weighing on a Sartorius Ultramicro balance (with a 0.1 µg detection limit) in a clean room with controlled temperature ($21 \pm 1.5\,^{\circ}C$) and humidity (35 ± 5 % RH), following EPA protocols. Potential static build-up is eliminated using an electrostatic blower. Absolute mass values are converted to mass concentration of $PM_{2.5}$, PM_{10} and $PM_{10-2.5}$ by dividing accumulated filter mass divided by total average air flow (with units of $\mu g\,m^{-3}$). The 2σ combined pre and post-weighing errors average 3.8 µg, or 0.7 $\mu g\,m^{-3}$ for 24 h of air sampling. This replicate weighing uncertainty corresponds to a precision of 4 % for typical filter loadings of about 100 µg.

Particle light absorbance of PTFE filters is measured using a Diffusion Systems EEL 43M smoke stain reflectometer (SSR), which acts as a surrogate for black carbon (Quincey et al., 2009). The SSR measurements are calibrated to thermal optical reflectance elemental carbon measurements on pre-fired quartz filters collected with a collocated Harvard Impactor at each measurement site as recommended in Cyrys et al. (2003).

Filters are then cut in half with a ceramic blade. Soluble ion extraction is performed by sonication on one half of the filter with 3 mL of distilled water and 4 % isopropyl alcohol as described by Gibson et al. (2013a, b). Ionic species (i.e. F^-, Cl^-, NO_2^-, NO_3^-, SO_4^{2-}, PO_4^{3-}, Li^+, K^+, Na^+, NH_4^+, Ca^{2+} and Mg^{2+}) are separated and quantified by ion chromatography (ICS-1000, Dionex). Major ions species have detection limits

of $\sim 10\,\mathrm{ng\,m^{-3}}$ depending on collected particle masses and potential matrix contaminants.

The other half of the filter is digested in 10 % nitric acid to extract water-insoluble metals (Celo et al., 2010) . Trace metals are detected through inductively coupled plasma-mass spectrometry (ICPMS Thermo Scientific X-Series 2). The detection limit for dissolved trace metals depends on the element and sample matrix. For a 3 mL extraction volume per filter, the 21 detectable metals relevant to atmospheric processes are ($3\,\sigma$, in $\mathrm{pg\,m^{-3}}$) Si(78), Al (10), Ti (1), V (1), Cr (1), Mn (2), Fe(18), Co(1), Ni (1), Cu (2), Zn (2), As (1), Se (3), Ag(1), Cd (1), Sn(2), Sb(5), Ba(1), Ce(1), Pb (1) and U(1).

3.3 Nephelometry

The AirPhoton IN100 nephelometer is a continuous sampling, optically based device measuring total particulate scatter b_{sp} at red (632 nm), green (532 nm) and blue (450 nm) wavelengths over the angular range 7° to 170°. The AirPhoton nephelometer records backscatter (b_{bks}) information between 92° and 170°. Light emitting diodes (LEDs) supply the light source. Total scatter is related to total aerosol concentration while backscatter provides information on aerosol size distribution. The forward and backscattering measurements are made independently. Internal sensors measure the incoming air stream for ambient relative humidity, temperature and pressure. The nephelometer is a separate module from the air sampler and mounts to a support stand. The inlet is a 10 cm length of copper tubing ending with a plastic bug screen. Light-scatter and backscatter are logged every 15 s on a 2 gigabyte SD card in units of inverse megameters ($\mathrm{Mm^{-1}}$). Ambient air temperature, humidity, and pressure are also recorded at the same frequency on the memory card. The nephelometer is not heated nor is any size cut introduced and the absence of a dryer also reduces concerns about evaporation of semivolatile components. The ambient nature of the measured aerosol scatter makes these results consistent with aerosol scatter observed by satellite.

The nephelometer light scattering by particulates, b_{sp}, is reported as one-hour averages, $b_{sp,1\,h}$. Hourly dry aerosol scatter component, $b_{sp,dry\text{-}1\,h}$, is calculated as

$$b_{sp,dry\text{-}1\,h} = \frac{b_{sp,1\,h}\{RH < RH_{max}\}}{f_m(RH)} \quad (1)$$

The term RH_{max} signifies the exclusion of b_{sp} values for which the hourly averaged humidity exceeds a threshold initially taken as 80 % to reduce uncertainty in the effects of aerosol water given the uncertain nature of aerosol composition. The hygroscopic mass correction factor $f_m(RH)$ accounts for the uptake of water in aerosols. The humidity correction factor is given here by $f_m(RH) = 1 + \frac{\rho_w}{\rho_s} \cdot \kappa \cdot RH/(100 - RH)$, where ρ_w and ρ_s are the density of water and the dry aerosol, respectively. The aerosol volume growth estimate of the water content of aerosols can often be within experimental error (Kreidenweis et al., 2008). Based on our studies from Beijing and the United States we have found that a hygroscopicity parameter $\frac{\rho_w}{\rho_s}\kappa = 0.2$ represents a variety of aerosol types. This value is similar to that obtained for urban aerosols (Padró et al., 2012). Future work will refine the $f_m(RH)$ calculation for specific site locations via measured water-soluble ion concentrations and their associated hygroscopicity.

3.4 Merging aerosol filter and nephelometer data

Hourly nephelometer scatter as measured by the nephelometer, is approximately proportional to $PM_{2.5}$ mass (Chow et al., 2006), however absolute mass predictions depend on aerosol composition. We therefore relate relative fluctuations in dry aerosol scatter from Eq. (1) anchored to an absolute filter mass ($\overline{PM}_{2.5,dry,9\,d}$):

$$PM_{2.5,dry-1\,h} = \overline{PM}_{2.5,dry,9\,d}\frac{b_{sp,dry\text{-}1\,h}}{\overline{b_{sp,dry,9\,d}}} \quad (2)$$

The "dry" subscript refers to the low humidity conditions at which filters are weighed (Sect. 3.2.2). Quantities with bars above them are averages for the given length of

time, hence $\overline{b}_{sp,dry,9\,d}$ represents the 9 day mean of dry aerosol scatter. Eq. (2) was evaluated in a simulated test using IMPROVE 24 h $PM_{2.5}$ measurements and nephelometer scatter, and compared with EPA hourly tapered element oscillating microbalance $PM_{2.5}$. The hourly nephelometer $PM_{2.5}$ prediction accuracy was 1 $\mu g\,m^{-3}$ + 17 % for three North American sites and for Beijing (cf. Appendix A5).

3.5 Ongoing evaluation

The evaluation of the SPARTAN network is an ongoing task. Martins et al. (2014) describe and evaluate of the AirPhoton instrumentation in detail. Appendix B describes an initial pilot study from university sites in Beijing, Halifax and Atlanta. Appendix B5 describes a Harvard Impactor being circulated across sites for intercomparison. We have begun a nephelometer and $PM_{2.5}$ composition intercomparison at Mammoth Cave, Kentucky between SPARTAN and IMPROVE. Measurements will begin in late summer at the EPA South Dekalb supersite near Atlanta, USA to compare with hourly federal reference method beta attenuation monitor (FRM-BAM) $PM_{2.5}$ measurements. Information gleaned from these assessments is being used to refine instrumentation and protocols.

4 Initial results

4.1 Initial temporal variation of $PM_{2.5}$ / AOD in Beijing

The ratio of ground-level $PM_{2.5}$ and AOD is fundamental in inferring $PM_{2.5}$ from satellite observations of AOD. We introduce initial measurements of this ratio to provide an example of the type of information SPARTAN can provide. The hourly $PM_{2.5}$ inferred from Eqs. (1) and (2) is related to AERONET AOD columns to create a time series of η, which was defined by van Donkelaar et al. (2010) as the ratio of 24 h $PM_{2.5}$ to AOD at satellite overpass time (AOD_{sat}, taken here as AOD averaged from 10:00 to

14:00 LT). AOD is interpolated to 550 nm via the angstrom exponents measured as part of AERONET.

$$\eta = \frac{PM_{2.5,24\,h}}{AOD_{sat}} \tag{3}$$

The top panel of Fig. 3 shows daily-varying concentrations of η in Beijing, China for select months in 2013–2014. Daily $PM_{2.5}$ ranged from 7–228 $\mu g\,m^{-3}$ while AOD_{sat} ranges from 0.05–3.8 during the measured sampling periods. We observe that the $PM_{2.5}$ / AOD ratio exhibits dramatic daily variation of more than an order of magnitude as well, ranging from below 50 $\mu g\,m^{-3}$ to above 900 $\mu g\,m^{-3}$. However, the variability of η is explained by neither AOD nor $PM_{2.5}$ alone; the R^2 between η and 1 / AOD_{sat} is 0.16 while between η and $PM_{2.5,24\,h}$ is 0.07.

Further insight into the variation in η is offered by decomposing η into three terms:

$$\eta = \left(\frac{b_{sp,sat}}{AOD_{sat}}\right)\left(\frac{b_{sp,24\,h}}{b_{sp,sat}}\right)\left(\frac{PM_{2.5,24\,h}}{b_{sp,24\,h}}\right) \tag{4}$$

The first term is a function of the aerosol vertical profile and describes the ratio of ground-level aerosol scattering (at satellite overpass time, $b_{sp,sat}$) to columnar aerosol optical depth (AOD_{sat}). The second term describes the diurnal variation in near-ground scattering during satellite overpass time vs. over the entire 24 h day ($b_{sp,24\,h}$) and requires only the nephelometer. Raw nephelometer scatter is interpolated to 550 nm via the angstrom exponents calculated from nephelometer measurements. Hourly scatter values for which RH > 80 % (Eq. 1) or $b_{sp,532} > 1300\,Mm^{-1}$ (nonlinear regime) are also omitted. The third term is the inverse of the mass scattering efficiency and related to aerosol composition. The product of the three terms in Eq. (4) will cancel to yield Eq. (3).

Figure 3 also shows the time series for these three terms. We find that η is most strongly related to the aerosol scattering vertical profile (first term Eq. 4, $R^2_{T1} = 0.57$).

In contrast, η is weakly related to diurnal variation in atmospheric scattering (second term Eq. (4), $R^2_{T2} = 0.20$) and to the mass scattering efficiency (third term Eq. 4, $R^2_{T3} = 0.005$). Given that hourly $PM_{2.5}$, as defined in Eq. (2), depends on b_{sp} in SPARTAN, we also interpreted η_{BAM} as inferred with an external $PM_{2.5}$ measurement via a Beta Attenuation Monitor on the roof of the US Embassy 8 km southeast from Tsinghua University. Relationships of η_{BAM} with the three terms in Eq. (4) show the same essential features such that $R^2_{T1} = 0.52$, $R^2_{T2} = 0.12$, $R^2_{T3} = 0.04$. The majority of the daily variance in η in Beijing is therefore explained by the relative ground-to-column vertical profile of aerosol scattering. Future work will examine these relationships at other sites, temporally, in detail.

The time periods selected for Fig. 3 represent two separate protocols for air filter sampling. February–April 2013 was part of the initial pilot study with filters exchanged every 24 h. The December 2013–January 2014 period was part of the "beta" testing of the 9 day sampling period. It is noteworthy that the relationship of η with the three terms in Eq. (4) remains comparable for both time periods despite the extended filter sampling protocol in the latter period.

4.2 Global variation in $PM_{2.5}$ / AOD

We have begun to examine factors affecting the global variation in η in order to explore how satellite AOD relates to $PM_{2.5}$ in different regions of the world. Table 2 contains mean values of η (and related measurements) across SPARTAN sites. Mean $PM_{2.5}$ varied from 3.2 $\mu g\,m^{-3}$ (Dalhousie) to 101 $\mu g\,m^{-3}$ (IIT Kanpur) while mean AOD across sites varied from 0.09 (Dalhousie, Emory) to 0.9 (Dhaka). The factor of 6 spatial variation of η across all sites is weaker than either the spatial variation in $PM_{2.5}$ or the daily variation in η. There appears to be a tendency for η to increase with $PM_{2.5}$; the $PM_{2.5}$ / AOD ratio is better related to mean $PM_{2.5}$ ($R^2 = 0.51$) than AOD_{sat} ($R^2 = 0.01$). We again used Eq. (4) to understand the factors affecting η. Excluding Bandung, which experienced a volcanic eruption during the test phase, η appears to be closely related

to the ratio of ground-level atmospheric scattering to column AOD (term 1; $R^2 = 0.75$) moderately related to the mass extinction efficiency (term 3; $R^2 = 0.40$), and weakly related to diurnal variation (term 2; $R^2 = 0.02$). The sub-Saharan site of Ilorin had the lowest values of η, reflecting the influence of coarse mineral dust as indicated by low measured $PM_{2.5}$ / PM_c ratios. Locations with elevated $PM_{2.5}$ generally have higher $b_{sp,sat}$ / AOD_{sat} ratios, implying a larger fraction of aerosol scattering is near the surface. Dhaka, however, had a similar ratio (i.e. only 40 % higher) compared with Halifax as well as similar η values (4 % higher) despite tenfold higher $PM_{2.5}$ levels, implying a pronounced aerosol scattering layer above Dhaka. Coarse PM also plays a role in Dhaka. The high mass scattering efficiency at Bandung was observed after the eruption and appears to reflect volcanic sulfate particles grown in high relative humidity. We caution these results are preliminary but demonstrate the potential to understand the relation of $PM_{2.5}$ with AOD at a variety of sites around the world.

Table 2 also contains an initial comparison of the measured values of η vs. the simulated values from the GEOS-Chem model that van Donkelaar et al. (2010) used to produce global satellite-based $PM_{2.5}$ estimates. We include in this comparison measurements from the two global locations (Taiwan and Mexico City) that had nearly collocated (within 3 km) AOD and $PM_{2.5}$ measurements. Comparison of mean $PM_{2.5}$ and AOD reveals that in most locations measured ratios were within range of GEOS-Chem estimates, though many are at the upper end of this range, including in Bandung, Kanpur, Taiwan, Halifax, and Beijing. The Bandung site data was well above the GEOS-Chem ratio, however a volcanic eruption during sampling likely played some role. Future work will conduct a more rigorous comparison for identical time series.

Additional information from SPARTAN measurements is being prepared for detailed analysis. Already we see that sulfate concentrations varied by a factor of 8 across sites. Nitrate concentrations in Beijing were an order of magnitude higher than any other site. Cations offer additional information about sea salt and fine dust. The angstrom exponent and the backscatter fraction measured by the nephelometer offer the prospect to retrieve aerosol size following Kaku et al. (2014).

5 Summary and outlook

We outlined the development of a grass-roots global network designed to evaluate and enhance satellite-based estimates of fine particulate matter for application in health effects research and risk assessment. Priority locations were chosen in densely populated areas outside the present reach of North American and European monitoring networks. The network is designed to assess the global heterogeneity between $PM_{2.5}$ and columnar aerosol optical depth (AOD). Data are collected to account for sampling done at specific overpass times and for the frequency of cloud-free conditions. Measurements from existing networks were used to develop and evaluate network design.

The network is comprised initially of two highly autonomous instruments, a three-wavelength nephelometer and an air filter sampler that measures $PM_{2.5}$ and PM_{10}. The nephelometer reports measurements continuously while the filters report as 9 day averages of particulate dry mass. A key feature of SPARTAN is that sites are collocated with AOD measurements via sun photometer instruments such as through the AERONET network.

The SPARTAN sampling strategy is designed to cost-effectively measure long-term and hourly $PM_{2.5}$ concentrations. Filter cartridges operate in the field for two months before being exchanged with a clean cartridge. Each filter cartridge holds eight coarse-mode and eight fine-mode filters with one set as a travelling blank. Each non-blank filter collects PM for one diurnal cycle during the course of the sampling period. Sampling ends in the morning when temperatures tend to be low to reduce loss of semivolatiles associated with active warm airflow across filters. $PM_{2.5}$ is collected on PTFE filters, which are analysed for total fine particulate mass (gravimetric), black carbon, water-soluble ion speciation (ion chromatography), and metal concentrations (inductively-coupled plasma mass spectrometry). All filters are analyzed in one central location under a verified single protocol to ensure similar analysis for filters from all locations. SPARTAN data is being made publicly available along with instrument protocols at spartan-network.org.

An initial analysis of SPARTAN measurements was conducted. We found a pronounced variability of more than an order of magnitude in the relation of columnar AOD to ground-level $PM_{2.5}$. This variability was analyzed in terms of the factors measured within SPARTAN, including the ratio of ground-level scatter to AOD, the diurnal variation in ground-level scatter, and the mass scattering efficiency. Data in Beijing indicate that the temporal variation in $PM_{2.5}$ / AOD is driven primarily by the vertical profile in aerosol scattering. Spatial variation in $PM_{2.5}$ across sites ranged from $< 10\,\mu g\,m^{-3}$ to $> 100\,\mu g\,m^{-3}$. Variation in $PM_{2.5}$ / AOD between sites is weaker (by a factor of 3) than temporal variation at a given site but is also driven by the aerosol vertical profile and to a lesser extent scattering mass efficiency.

Assessment of instrumentation and protocols is an ongoing task. Ongoing work includes (1) further testing of AirPhoton instrumentation at the EPA supersite in Atlanta and at the Mammoth Cave IMPROVE site (2) the expansion of instrument sites to other sun photometer locations and (3) implementation of a cyclone $PM_{2.5}$ inlet in order to obtain a sharper $PM_{2.5}$ cut.

Future work will explore utilising the multi-wavelengths capability of the nephelometer to improve $PM_{2.5}$ estimates by providing refined size distribution information. We are seeking opportunities to expand the instrumentation to create supersites at some SPARTAN locations for related process studies. Collocation with lidar sites would be valuable. In late 2014 the NERC Airborne Science Research and Survey Facility will conduct aircraft vertical profiles over four SPARTAN sites (Kanpur, India; Dhaka, Bangladesh; Manila, Philippines; Bandung, Indonesia) and near one other (Hanoi, Vietnam). SPARTAN is focused on the health applications of all principal measurements. Nonetheless, this network should also provide a unique dataset for climate studies and regional $PM_{2.5}$ source appointment.

Appendix A: Evaluation of SPARTAN sampling strategy

A1 Representativeness of a point for an urban area

We evaluated the degree to which the location of a single aerosol monitoring station is affected by its location within a city by comparing all site pairings (where n sites creates $(n^2 - n)/2$ pairings) for two dense measurement networks in Asia. The left panel in Fig. A1 shows the coefficient of variation (R^2) between daily $PM_{2.5}$ measured with Beta Attenuation Monitors at 36 sites in Beijing and 76 sites in Taiwan. The coefficient of variation tends to unity for collocated instruments. Eighty percent of Beijing station pairings separated by less than 10 km showed $R^2 > 0.90$ while 73 % of Taiwan stations had $R^2 > 0.90$. The right panel is the relative difference (RD) in annual 24 h mean $PM_{2.5}$ measured at site pairs i and j such that $RD_{ij} = 2 \cdot (PM_{2.5}{}^{i} - PM_{2.5}{}^{j})/(PM_{2.5}{}^{i} + PM_{2.5}{}^{j})$. The relative errors were symmetric around zero. Station pairings separated by less than 10 km have mean errors of 12 % in Beijing and 17 % in Taiwan. Therefore single monitoring stations, if properly installed and calibrated, can well represent a satellite observation area on the order of 100 km^2.

A2 Losses of aerosol ammonium nitrate

Ammonium nitrate (NH_4NO_3) $PM_{2.5}$ was generated with a mean diameter of 400 nm using a TSI Constant Output Atomizer (model 3076), then captured on preweighed PTFE filters at 23 °C. The mass of captured NH_4NO_3 on filters was recorded and filters were returned to the cartridge. The cartridge was then placed in an insulated case held constant at 31 °C. Four filters actively sampled indoor air for 5 h at 4 lpm in a heated environment and then were exposed to 15 h in the heated environment without airflow. Three other filters sat in the heated environment without airflow during this same period. Following this procedure, the mean hourly rate of mass lost from the filters with active airflow was 3.4 (± 0.2) % compared to 0.16 (± 0.09) % for the filters without active airflow. Moderate loss of NH_4NO_3 can be expected from the PTFE filters while warm

air is flowing over the filters, but is otherwise slow. Further evidence that ammonium nitrate are retained is that our measured NO_3^-/SO_4^- ratio at Tsinghua 0.74 (± 0.32) (Table 2) is comparable to previous measurements of 0.64 (± 0.56) by Yang et al. (2011) in Beijing.

A3 Assessment of temporal sampling strategy

We examined how well different sampling approaches represent annual mean $PM_{2.5}$ concentrations by using hourly measurements of $PM_{2.5}$ from ~ 100 EPA sites across the United States over a year. At each of these locations a beta attenuation monitor (BAM) or tapered element oscillating microbalance (TEOM) recorded hourly $PM_{2.5}$ concentrations. We "sampled" these hourly concentrations at intervals of 1, 2, 3, 4, 6, 8, 12, and 24 h while comparing with uninterrupted sampling. Figure A2 shows the percent error obtained from different sampling approaches.

The green line shows 1-in-X day sampling errors increase rapidly with decreasing duty cycle. The red line shows that sampling every day at the same time of day has reduced errors compared with 1-in-X day sampling. The blue line shows staggered sampling. For example a 3 h interval (12.5 % sampling) means day 1 samples from 00:00 to 03:00 LT, day 2 is sampled 03:00 to 06:00 LT, et cetera until day 8 is reached. Shorter sampling intervals require more days to reach a 24 h average. Staggered sampling reduced representativeness errors compared with single-day sampling. Sampling error increases slowly as duty cycle decreases. The red line shows that sampling 3 h at the same time each day results in a 40 % daily mean error, however the expected error for 3 h staggered intervals over an 8 day mean was much lower, at 13 %. Thus we choose staggered sampling to increase the representativeness of mean $PM_{2.5}$ measurements.

A4 Modifying protocol for high $PM_{2.5}$ concentrations

Six consecutive 9 day tests at the Atlanta site measured the loss of airflow through the AirPhoton instrument. Initially filters collected aerosols without any change in flow, however a 10 % loss of airflow became apparent when more than 160 µg of coarse aerosol material deposited on the capillary pore surface (i.e. 50 µg cm^2). Given a flow rate of 4 L min^{-1}, this is equivalent to a maximum sustainable PM concentration of 28 µg m^{-3}. We avoid exceeding a median threshold of half this value; sites with ambient PM_c concentrations less than 14 µg m^{-3} are sampled for 160 min a day over 9 days (i.e. 24 h total; 100 % duty). Elsewhere, the daily sampling duration (% duty) follows Eq. (A1) to avoid collecting more than 160 µg of PM_{coarse}.

$$\%\,\text{Duty} \approx \begin{cases} 100\,\% & \overline{PM_c} \le 14\,\mu g\,m^{-3} \\ \frac{160\,\mu g}{2[\overline{PM_c}]\cdot V_{samp}} \cdot 100\,\% & \overline{PM_c} > 14\,\mu g\,m^{-3} \end{cases} \quad \text{(A1)}$$

V_{samp} is the volume of air passing through the filter in 24 h (5.76 m^3 for 24 h at 4 L min^{-1}). Initial $\overline{PM_c}$ concentrations are estimated from available data. When coarse-mode ground-level aerosol is unknown, a doubling of satellite-derived $PM_{2.5}$ is used in Eq. (A1) as an initial estimate. Actual duty cycles are being be refined as more SPARTAN data are acquired.

A5 Expected daily $PM_{2.5}$ errors during satellite overpass times

We examined the quality of hourly $PM_{2.5}$ inferred from Eq. (1) for 24 h periods and during typical satellite daytime overpass times (10:00 to 14:00 LT). This test case was based on three IMPROVE network sites near EPA sites. The IMPROVE sites provide hourly nephelometer (b_{sp}) readings while EPA sites provided hourly $PM_{2.5}$ mass using a tapered elemental oscillating microbalance (TEOM) instrument. We discarded all b_{sp} values for which hourly RH > 80 %. We identified three EPA and IMPROVE sites that

were (a) within 50 km of each other, (b) had less than a 100 m elevation difference and (c) had at least one year of sampling overlap. We compared $PM_{2.5}$ predictions vs. hourly TEOM for both satellite and 24 h averages and attempted to account for water uptake mass using Eq. (1). Uniquely for this analysis we defined $\overline{PM}_{2.5,dry}$ in Eq. (2) as a 24 h average of the TEOM. By substituting gravimetric masses for this average we isolated the error contribution from Eq. (1) and ignore inter instrument bias. TEOM and BAM instruments have inherent hourly 1σ precisions of 2 µg m^{-3} and daily precisions of 1 µg m^{-3} (Thermo Scientific, 2013). An offset of 1 µg m^{-3} was used to account for instrument uncertainties.

Figure A3 gives the results from all three EPA/IMPROVE-paired locations. The slope is near unity for both all-day and satellite hours ($m_{24\,h}$ = 0.96, m_{sat} = 0.97). The mean 24 h error is 16.8 %. Some errors are due to EPA and IMPROVE sites not being collocated. Uncertainties in water uptake of aerosols also contribute to error. We find increasing relative errors as we introduce higher RH cutoffs; increasing the RH curtoff from 80 % to 90 % using IMPROVE data increases error by 10–20 %.

Table A1 includes the errors obtained from the three US locations. Moving from 24 h to satellite overpass times reduces average all-day errors from 1 µg m^{-3} + 17 % (24 h) to 1 µg m^{-3} + 12 % for satellite overpass hours. Midday hours have lower relative humidity.

Appendix B: Pilot project air sampling and weighing protocol

B1 Test sites and collocated instruments

Three test sites were chosen to represent locations of high $PM_{2.5}$ (Tsinghua University; Beijing, China), moderate $PM_{2.5}$ (Emory University; Atlanta, GA, United States) and low $PM_{2.5}$ (Dalhousie University; Halifax, Canada) concentrations. For each site the AirPhoton air sampler and nephelometer were collocated with at least one filter-based and light-scattering instrument. Halifax had two federal reference method (FRM)

instruments on site, the Partisol 2025 ($PM_{2.5}$: EQPS-0509-179, PM_{coarse}: EQPS-0509-180, Themo Scientific) and the BAM (EQPM-0308-170, Met One). Beijing had one FRM on site: the TEOM 1400 (EQPM-0609-181). We compare with BAM data as reported from the US Embassy (twitter.com/beijingair) located 8 km southeast of Tsinghua University. Table A2 contains a full listing of intercomparison instruments.

B2 Nephelometer trending

The AirPhoton nephelometer was collocated with a DustTrak, Aurora, and Dylos instruments in Halifax, a GRIMM monitor in Atlanta, and DustTrak instrument in Beijing. Measurements with RH > 80 % were excluded. Good correlation (R^2 = 0.80 to 0.98) was found for all three sites at red, green, and blue wavelengths compared to 5 to 15 min averages of reference instruments.

In Beijing the prototype AirPhoton nephelometer signal saturated during extreme pollution events ($PM_{2.5} > 400\,\mu g\,m^{-3}$). Light scattering performance returned to normal after these events. The Beijing pollution episodes from January–March 2013 were exceptional but modifications to the nephelometer to accommodate up to $2000\,Mm^{-1}$ dry aerosol scattering have been implemented to accommodate these extreme cases.

B3 Assembled $PM_{2.5}$ filter results from all three cities

Figure A4 illustrates the $PM_{2.5}$ masses as obtained by filter weight from the three cities Halifax, Atlanta and Beijing. Each site used a different reference instrument. For the purpose of estimating global $PM_{2.5}$ there is some precedent for combining data from various reference sources (Brauer et al., 2011). After merging our data sets from all three cities the resulting coefficient of variation is 0.96. The combined slope is 0.75 ± 0.02 with a negligibly small intercept of $-0.08\,\mu g\,m^{-3}$. These differences are similar to previous comparison between approved FRM and federal equivalence method (FEM) instruments (Cyrys et al., 2001; Hains et al., 2007; Liu et al., 2013; Motallebi et al., 2003; Schwab et al., 2006). Nonetheless, the low slope implies that the AirPhoton

prototype underestimated $PM_{2.5}$ with respect to reference instruments. The nuclepore filters provide only an approximate $PM_{2.5}$ size cut. At each SPARTAN site a Harvard Impactor is used to assess the location-specific effects of the size cut until a $PM_{2.5}$ cyclone inlet becomes available for AirPhoton instruments.

In Halifax the slope of the AirPhoton $PM_{2.5}$ estimates with respect to the Partisol was 1.26 ± 0.12. The moderate correlation (R^2 = 0.55) is likely due to the low mean $PM_{2.5}$ concentrations ($4.4\,\mu g\,m^{-3}$) over the January to March sampling period. These concentrations are at the low end of annual averages recorded for any populated area in the world (Brauer et al., 2011). The Halifax AirPhoton site underreported PM_{coarse} with respect to Partisol, at 0.74 ± 0.06 (R^2 = 0.70). In Atlanta the slope of $PM_{2.5}$ was 0.88 ± 0.08 with respect to a personal environmental monitor (PEM) reference filter. The R^2 of the two data sets is 0.82.

The Beijing air samples followed a reduced sampling protocol. The city of Beijing experienced very high levels of $PM_{2.5}$ during this pilot study, with hourly concentrations passing $500\,\mu g\,m^{-3}$ and daylong averages occasionally above $200\,\mu g\,m^{-3}$. Sampling was decreased to 10 % of every hour (for a total of 2.4 h per day) to avoid filter clogging. The reported $PM_{2.5}$ values correlated well (R^2 = 0.87) with the Laoying. The slope is low compared with the Laoying (0.77) as well as the BAM (0.64) but close to the TEOM (0.93); the latter is known to underreport $PM_{2.5}$ due to semivolatile losses (Cyrys et al., 2001).

B4 Hourly $PM_{2.5}$ inferred in Beijing vs. BAM instrument

Figure A5 shows hourly $PM_{2.5}$ at Tsinghua University between 23 February and 29 March 2013. Daily $PM_{2.5}$ concentrations are defined as 24 h averages reported by the BAM, $\langle PM_{2.5}\rangle_{BAM}$, to eliminate sources of error dependent on dry mass calculations. Green nephelometer (532 nm) total scatter values and humidity were used to infer hourly $PM_{2.5}$ estimates using Eq. (1). These values were normalized every 24 h (excluding those hours for which humidity is above 80 %) and compared with the hourly

BAM data. We focused on the predictive ability of the nephelometer for hourly $PM_{2.5}$. Green (532 nm) scatter above 1300 Mm^{-1} was screened, as higher aerosol concentrations were non-linear. Promising correlations are found with 24 h BAM fine mass ($R^2_{24\,h,hourly}$ = 0.88) and satellite overpass times averages ($R^2_{sat,hourly}$ = 0.94) despite the 8 km of separation between the BAM and nephelometer. The lower correlation of the all-day relationship is likely due slight non-linearities for $PM_{2.5}$ concentrations above 400 $\mu g\,m^{-3}$. The standard deviation (1σ)T envelope compared with the RMA line for BAM-referenced $PM_{2.5}$ is 1 $\mu g\,m^{-3}$ + 17 % for both all-day and satellite-only values. Mass differences for the Beijing pilot test were comparable to the multi-year trial estimates in the United States (Table A1). A sensitivity test that extended the reference period to 24 h $PM_{2.5}$ means (with scatter and $PM_{2.5}$ averaged over 9 day spans) resulted in similar $PM_{2.5}$ discrepancies, at 1 $\mu g\,m^{-3}$ + 16 % but with reduced variance ($R^2_{24\,h,daily}$ = 0.94).

B5 Additional measurements

A Harvard Impactor is used to assess the performance of size cut of AirPhoton instruments for the conditions at their sampling locations until a $PM_{2.5}$ cyclone inlet becomes available for the AirPhoton sampling station. These instruments are straightforward to operate and pre-programmed sampling pump protocols are provided. Harvard Impactors are known to provide an accurate measurement of $PM_{2.5}$ (Babich et al., 2000), and two are being shipped to each site for a three weeks of daily collocated sampling. The AirPhoton instrument operates on a daily cycle for expediency during this intercalibration period. Further assessment for difference seasons will be conducted using the cyclone inlet. After sampling, the PTFE and quartz filters are returned to Dalhousie University for analysis including post-weighing. Quartz filters are also collected for thermal analysis of elemental carbon via an OC/EC analyser (Sunset Laboratory), and used to correct PTFE reflectance via the Smoke Stain Reflectometer instrument.

Acknowledgements. National Sciences and Engineering Research Council (NSERC) of Canada supported this work. We are grateful to many others who have offered helpful comments and advice on the creation of this network including Jay Al-Saadi, Ross Anderson, Kalpana Balakrishnan, Len Barrie, Sundar Christopher, Matthew Cooper, Jim Crawford, Doug Dockery, Jill Engel-Cox, Greg Evans, Markus Fiebig, Allan Goldstein, Judy Guernsey, Ray Hoff, Rudy Husar, Mike Jerrett, Michaela Kendall, Rich Kleidman, Petros Koutrakis, Glynis Lough, Doreen Neil, John Ogren, Norm O'Neil, Jeff Pierce, Thomas Holzer-Popp, Ana Prados, Lorraine Remer, Sylvia Richardson, and Frank Speizer. The site at IIT Kanpur is supported in part by National Academy of Sciences and USAID. The views expressed here are of authors and do not necessarily reflect of NAS or USAID.

References

Ackermann, J.: The extinction-to-backscatter ratio of tropospheric aerosol: a numerical study, J. Atmos. Ocean. Technn., 15, 1043–1050, doi:10.1175/1520-0426(1998)015<1043:TETBRO>2.0.CO;2, 1998.

Anenberg, S. C., Horowitz, L. W., Tong, D. Q., and West, J. J.: An estimate of the global burden of anthropogenic ozone and fine particulate matter on premature human mortality using atmospheric modeling., Environ. Health Perspect., 118, 1189–1195, 2010.

Center for International Earth Science Information Network: CIESIN – Columbia University, and Centro Internacional de Agricultura Tropical – CIAT, 2005, Gridded Population of the World, Version 3 (GPWv3): Population Density Grid, Palisades, NY: NASA Socioeconomic Data and Applications Center (SEDAC), doi:10.7927/H4XK8CG2, last access: 1 April 2014.

Babich, P., Davey, M., Allen, G., and Koutrakis, P.: Method comparisons for particulate nitrate, elemental carbon, and $PM_{2.5}$ mass in seven U.S. cities, J. Air Waste Manage., 50, 1095–1105, doi:10.1080/10473289.2000.10464152, 2000.

Bell, M. L., Morgenstern, R. D., and Harrington, W.: Quantifying the human health benefits of air pollution policies: review of recent studies and new directions in accountability research, Environ. Sci. Policy, 14, 357–368, doi:10.1016/j.envsci.2011.02.006, 2011.

Brauer, M., Amann, M., Burnett, R. T., Cohen, A., Dentener, F., Ezzati, M., Henderson, S. B., Krzyzanowski, M., Martin, R. V., Van Dingenen, R., van Donkelaar, A., and Thurston, G. D.:

Exposure assessment for estimation of the global burden of disease attributable to outdoor air pollution, Environ. Sci. Technol., 46, 652–660, doi:10.1021/es2025752, 2011.

Celo, V., Dabek-Zlotorzynska, E., Mathieu, D., and Okonskaia, I.: Validation of a simple microwave-assisted acid digestion method using microvessels for analysis of trace elements in atmospheric $PM_{2.5}$ in monitoring and fingerprinting studies, Open Chem. Biomed. J., 3, 143–152, doi:10.2174/1875038901003010143, 2010.

Chen, H., Goldberg, M. S., and Villeneuve, P. J.: A systematic review of the relation between long-term exposure to ambient air pollution and chronic diseases, Rev. Environ. Health, 23, 243–297, 2008.

Chow, J. C.: Measurement methods to determine compliance with ambient air quality standards for suspended particles, J. Air Waste Manage., 45, 320–382, doi:10.1080/10473289.1995.10467369, 1995.

Chow, J. C., Watson, J. G., Park, K., Lowenthal, D. H., Robinson, N. F., and Magliano, K. A.: Comparison of particle light scattering and fine particulate matter mass in central California, J. Air Waste Manage., 56, 398–410, 2006.

Crouse, D. L., Peters, P. A., van Donkelaar, A., Goldberg, M. S., Villeneuve, P. J., Bnon, O., Than, S., Afari, D. O., Jerrett, M., Pope, C. A., Brauer, M., Brook, J. R., Martin, R. V., Steib, D., and Burnett, R. T.: Risk of nonaccidental and cardiovascular mortality in relation to long-term exposure to low concentrations of fine particulate matter: a Canadian national-level cohort study, Environ. Health Persp., 120, 708–714, 2012.

Cyrys, J., Dietrich, G., Kreyling, W., Tuch, T. and Heinrich, J.: $PM_{2.5}$ measurements in ambient aerosol: comparison between Harvard impactor (HI) and the tapered element oscillating microbalance (TEOM) system, Sci. Total Environ., 278, 191–197, doi:10.1016/S0048-9697(01)00648-9, 2001.

Cyrys, J., Heinrich, J., Hoek, G., Meliefste, K., Lewne, M., Gehring, U., Bellander, T., Fischer, P., van Vliet, P., Brauer, M., Wichmann, H.-E., and Brunekreef, B.: Comparison between different traffic-related particle indicators: elemental carbon (EC), $PM_{2.5}$ mass, and absorbance, J. Expo. Anal. Env. Epid., 13, 134–143, 2003.

Fang, Y., Mauzerall, D., Liu, J., Fiore, A., and Horowitz, L.: Impacts of 21st century climate change on global air pollution-related premature mortality, Climatic Change, 121, 239–253, doi:10.1007/s10584-013-0847-8, 2013.

Friedl, L., Husar, R., and Falke, S.: GEO Task US-09-01a: Critical Earth Observations Priorities, Wahington, 2010.

Gibson, M. D., Heal, M. R., Li, Z., Kuchta, J., King, G. H., Hayes, A., and Lambert, S.: The spatial and seasonal variation of nitrogen dioxide and sulfur dioxide in Cape Breton Highlands National Park, Canada, and the association with lichen abundance, Atmos. Environ., 64, 303–311, doi:10.1016/j.atmosenv.2012.09.068, 2013a.

Gibson, M. D., Pierce, J. R., Waugh, D., Kuchta, J. S., Chisholm, L., Duck, T. J., Hopper, J. T., Beauchamp, S., King, G. H., Franklin, J. E., Leaitch, W. R., Wheeler, A. J., Li, Z., Gagnon, G. A., and Palmer, P. I.: Identifying the sources driving observed $PM_{2.5}$ temporal variability over Halifax, Nova Scotia, during BORTAS-B, Atmos. Chem. Phys., 13, 7199–7213, doi:10.5194/acp-13-7199-2013, 2013b.

Hains, J. C., Chen, L.-W. A., Taubman, B. F., Doddridge, B. G., and Dickerson, R. R.: A side-by-side comparison of filter-based $PM_{2.5}$ measurements at a suburban site: a closure study, Atmos. Environ., 41, 6167–6184, doi:10.1016/j.atmosenv.2007.04.008, 2007.

Hand, J. L., Schichtel, B. A., Pitchford, M., Malm, W. C., and Frank, N. H.: Seasonal composition of remote and urban fine particulate matter in the United States, J. Geophys. Res., 117, D05209, doi:10.1029/2011JD017122, 2012.

HEI: Outdoor Air Pollution and Health in the Developing Countries of Asia: a Comprehensive Review, Special Report 18, Boston, MA, 2010.

Heidam, N. Z.: Review: aerosol fractionation by sequential filtration with nuclepore filters, Atmos. Environ., 15, 891–904, doi:10.1016/0004-6981(81)90088-3, 1981.

Hitzenberger, R., Berner, A., Galambos, Z., Maenhaut, W., Cafmeyer, J., Schwarz, J., Müller, K., Spindler, G., Wieprecht, W., Acker, K., Hillamo, R., and Mäkelä, T.: Intercomparison of methods to measure the mass concentration of the atmospheric aerosol during INTERCOMP2000 – influence of instrumentation and size cuts, Atmos. Environ., 38, 6467–6476, doi:10.1016/j.atmosenv.2004.08.025, 2004.

Hoff, R. M. and Christopher, S. A.: Remote sensing of particulate pollution from space: have we reached the promised land?, J. Air Waste Manage., 59, 645–675, doi:10.3155/1047-3289.59.6.645, 2009.

Holben, B. N., Eck, T. F., Slutsker, I., Tanré, D., Buis, J. P., Setzer, A., Vermote, E., Reagan, J. A., Kaufman, Y. J., Nakajima, T., Lavenu, F., Jankowiak, I., and Smirnov, A.: AERONET – a federated instrument network and data archive for aerosol characterization, Remote Sens. Environ., 66, 1–16, doi:10.1016/S0034-4257(98)00031-5, 1998.

Hopke, P. K., Xie, Y., Raunemaa, T., Biegalski, S., Landsberger, S., Maenhaut, W., Artaxo, P., and Cohen, D.: Characterization of the Gent stacked filter unit PM_{10} sampler, Aerosol Sci. Technol., 27, 726–735, doi:10.1080/02786829708965507, 1997.

Husar, R. B., Husar, J. D., and Martin, L.: Distribution of continental surface aerosol extinction based on visual range data, Atmos. Environ., 34, 5067–5078, doi:10.1016/S1352-2310(00)00324-1, 2000.

John, W., Hering, S., Reischl, G., Sasaki, G., and Goren, S.: Characteristics of Nuclepore filters with large pore size – II. Filtration properties, Atmos. Environ., 17, 373–382, doi:10.1016/0004-6981(83)90054-9, 1983.

Kahn, R. A., Ogren, J. A., Ackerman, T. P., Bosenberg, J., Charlson, R. J., Diner, D. J., Holben, B. N., Menzies, R. T., Millier, M. A., and Seinfeld, J. H.: Aerosol data sources and their roles within PARAGON, B. Am. Meteorol. Soc., 85, 1511–1522, 2004.

Kaku, K. C., Reid, J. S., O'Neill, N. T., Quinn, P. K., Coffman, D. J., and Eck, T. F.: Verification and application of the extended Spectral Deconvolution Algorithm (SDA+) methodology to estimate aerosol fine and coarse mode extinction coefficients in the marine boundary layer, Atmos. Meas. Tech. Discuss., 7, 2545–2584, doi:10.5194/amtd-7-2545-2014, 2014.

Kong, S., Han, B., Bai, Z., Chen, L., Shi, J., and Xu, Z.: Receptor modeling of $PM_{2.5}$, PM_{10} and TSP in different seasons and long-range transport analysis at a coastal site of Tianjin, China, Sci. Total Environ., 408, 4681–4694, doi:10.1016/j.scitotenv.2010.06.005, 2010.

Kreidenweis, S. M., Petters, M. D., and DeMott, P. J.: Single-parameter estimates of aerosol water content, Environ. Res. Lett., 3, 35002, doi:10.1088/1748-9326/3/3/035002, 2008.

Laden, F., Schwartz, J., Speizer, F. E., and Dockery, D. W.: Reduction in fine particulate air pollution and mortality, Am. J. Resp. Crit. Care, 173, 667–672, doi:10.1164/rccm.200503-443OC, 2006.

Larson, T., Su, J., Baribeau, A.-M., Buzzelli, M., Setton, E., and Brauer, M.: A spatial model of urban winter woodsmoke concentrations, Environ. Sci. Technol., 41, 2429–2436, doi:10.1021/es0614060, 2007.

Lim, S. S., Vos, T., Flaxman, A. D., Danaei, G., Shibuya, K., Adair-Rohani, H., AlMazroa, M. A., Amann, M., Anderson, H. R., Andrews, K. G., Aryee, M., Atkinson, C., Bacchus, L. J., Bahalim, A. N., Balakrishnan, K., Balmes, J., Barker-Collo, S., Baxter, A., Bell, M. L., Blore, J. D., Blyth, F., Bonner, C., Borges, G., Bourne, R., Boussinesq, M., Brauer, M., Brooks, P., Bruce, N. G., Brunekreef, B., Bryan-Hancock, C., Bucello, C., Buchbinder, R., Bull, F., Burnett, R. T., Byers, T. E., Calabria, B., Carapetis, J., Carnahan, E., Chafe, Z., Charlson, F.,

Chen, H., Chen, J. S., Cheng, A. T.-A., Child, J. C., Cohen, A., Colson, K. E., Cowie, B. C., Darby, S., Darling, S., Davis, A., Degenhardt, L., Dentener, F., Des Jarlais, D. C., Devries, K., Dherani, M., Ding, E. L., Dorsey, E. R., Driscoll, T., Edmond, K., Ali, S. E., Engell, R. E., Erwin, P. J., Fahimi, S., Falder, G., Farzadfar, F., Ferrari, A., Finucane, M. M., Flaxman, S., Fowkes, F. G. R., Freedman, G., Freeman, M. K., Gakidou, E., Ghosh, S., Giovannucci, E., Gmel, G., Graham, K., Grainger, R., Grant, B., Gunnell, D., Gutierrez, H. R., Hall, W., Hoek, H. W., Hogan, A., Hosgood, H. D., Hoy, D., Hu, H., Hubbell, B. J., Hutchings, S. J., Ibeanusi, S. E., Jacklyn, G. L., Jasrasaria, R., Jonas, J. B., Kan, H., Kanis, J. A., Kassebaum, N., Kawakami, N., Khang, Y.-H., Khatibzadeh, S., Khoo, J.-P., et al.: A comparative risk assessment of burden of disease and injury attributable to 67 risk factors and risk factor clusters in 21 regions, 1990–2010: a systematic analysis for the Global Burden of Disease Study 2010, Lancet, 380, 2224–2260, 2012.

Lippmann, M.: Toxicological and epidemiological studies of cardiovascular effects of ambient air fine particulate matter ($PM_{2.5}$) and its chemical components: coherence and public health implications, Crit. Rev. Toxicol., 44, 299–347, doi:10.3109/10408444.2013.861796, 2014.

Liu, C.-N., Awasthi, A., Hung, Y.-H., Gugamsetty, B., Tsai, C.-J., Wu, Y.-C., and Chen, C.-F.: Differences in 24-h average $PM_{2.5}$ concentrations between the beta attenuation monitor (BAM) and the dichotomous sampler (Dichot), Atmos. Environ., 75, 341–347, doi:10.1016/j.atmosenv.2013.04.062, 2013.

Martins et al.: AirPhoton LLC, "Combined Sampling Station" instrument documentation available at: www.airphoton.com (last access: 1 June 2014), in preparation, 2014.

Motallebi, N., Taylor, C. A., Turkiewicz, K., and Croes, B. E.: Particulate matter in California: Part 1 – Intercomparison of several $PM_{2.5}$, PM_{10}–2.5, and PM_{10} monitoring networks, J. Air Waste Manage., 53, 1509–1516, doi:10.1080/10473289.2003.10466322, 2003.

Paciorek, C. and Liu, Y.: Limitations of remotely-sensed aerosol as a spatial proxy for fine particulate matter, Environ. Health Persp., 117, 904–909, doi:10.1289/ehp.0800360, 2009.

Padró, L. T., Moore, R. H., Zhang, X., Rastogi, N., Weber, R. J., and Nenes, A.: Mixing state and compositional effects on CCN activity and droplet growth kinetics of size-resolved CCN in an urban environment, Atmos. Chem. Phys., 12, 10239–10255, doi:10.5194/acp-12-10239-2012, 2012.

Parker, R. D., Buzzard, G. H., Dzubay, T. G., and Bell, J. P.: A two stage respirable aerosol sampler using nuclepore filters in series, Atmos. Environ., 11, 617–621, doi:10.1016/0004-6981(77)90114-7, 1977.

Punger, E. and West, J. J.: The effect of grid resolution on estimates of the burden of ozone and fine particulate matter on premature mortality in the USA, Air Qual. Atmos. Heal., 6, 563–573, doi:10.1007/s11869-013-0197-8, 2013.

Quincey, P., Butterfield, D., Green, D., Coyle, M., and Cape, J. N.: An evaluation of measurement methods for organic, elemental and black carbon in ambient air monitoring sites, Atmos. Environ., 43, 5085–5091, doi:10.1016/j.atmosenv.2009.06.041, 2009.

Schwab, J. J., Felton, H. D., Rattigan, O. V, and Demerjian, K. L.: New York State urban and rural measurements of continuous $PM_{2.5}$ mass by FDMS, TEOM, and BAM, J. Air Waste Manage., 56, 372–383, doi:10.1080/10473289.2006.10464523, 2006.

Thermo Scientific: 1405-D TEOM, Continuous Dichotomous Ambient Particulate Monitor, Thermo Fish. Sci. Inc., available at: http://www.thermoscientific.com/ecomm/servlet/productsdetail_11152___11960556_-1 (last access: 13 June 2013), 2013.

van Donkelaar, A., Martin, R. V, Brauer, M., Kahn, R., Levy, R., Verduzco, C., and Villeneuve, P. J.: Global estimates of ambient fine particulate matter concentrations from satellite-based aerosol optical depth: development and application, Environ. Health Persp., 118, 847–855, 2010.

WHO: Human exposure to air pollution, in: Update of the World Air Quality Guidelines World Health Organization, World Health Organization, Geneva, Switzerland, 61–86, 2005.

Yang, F., Tan, J., Zhao, Q., Du, Z., He, K., Ma, Y., Duan, F., Chen, G., and Zhao, Q.: Characteristics of PM2.5 speciation in representative megacities and across China, Atmos. Chem. Phys., 11, 5207–5219, doi:10.5194/acp-11-5207-2011, 2011.

Table 1. Site information for confirmed SPARTAN station locations.

Host name, Country	Site coordinates		Local pop. Density[a] (persons km^{-2})		Satellite $PM_{2.5}$ ($\mu g\,m^{-3}$)[b]	Temp.[c] (°C) [high/low]	Annual RH[c] (%)	Elev. (sea level) // height above ground (m)	Site description, location	Start Date
	Lat.	Long.	0.25° × 0.25°	10 km × 10 km						
Bandung, Indonesia	−6.888	107.610	1600	16 000	14	27/18	73	780 // 20	Rooftop of university building, urban	Jan 2014
CITEDEF, Argentina	−34.553	−58.509	1500	12 000	9	23/14	72	30 // TBD	TBD	TBD, late 2014
CSIR, Pretoria, South Africa	−25.751	28.279	1400	1900	12	23/13	58	1420 // TBD	TBD	TBD, late 2014
Dalhousie University, Canada	44.638	−63.594	500	1200	7	10/1	79	40 // 20	Rooftop of university building, suburban	Jan 2013
Emory University, USA	33.688	−84.290	890	1800	17	22/11	67	250 // 2	Emory supersite, ground-level, rural	Jan 2013
Indian Institute of Technology Kanpur, India	26.519	80.232	1000	3100	52	32/19	66	130 // 10	Rooftop near university airport, rural	Nov 2013
Mammoth Cave	37.132	−86.148	20	20	13	20/7	72	235 // 2	rural	Jun 2014
Manila Observatory, Philippines	14.635	121.077	9600	9100	16	31/23	79	60 // 10	Roof of Manila Observatory, suburban	Jan 2014
Manaus[d], Brazil	−2.594	−60.209	140	150	5	30/23	83	110 // TBD	TBD	TBD, late 2014
Nes Ziona, Israel	31.924	34.788	1600	1400	21	25/14	70	20 // TBD	TBD	TBD, mid 2014
Tsinghua University, China	39.977	116.380	3000	5600	96	17/7	57	60 // 20	Rooftop, urban	Jan 2013
University of Dhaka, Bangladesh	23.728	90.398	2900	51 000	42	31/22	75	20 // 20	University rooftop, urban,	Nov 2013
University of Ilorin, Nigeria	8.481	4.526	360	1100	17	27/25	57	330 // 10	University building rooftop, suburban	Apr 2014
Vietnam Academy of Science and Technology, Vietnam	21.048	105.801	3500	5700	46	26/21	80	10 // TBD	TBD	TBD, mid 2014

[a] Density determined using GPWv3 (Population Density Grid, 2010).
[b] van Donkelaar et al. (2010).
[c] Annual mean relative humidity and temperature data from www.weatherbase.com.
[d] Sampling protocol at Manaus is determined by the World Meteorological Organization Global Atmosphere Watch station.

Table 2. Spatial variation in η and related variables.

Host name, Country	Time span	Site coordinates		$PM_{2.5,24\,h}$ ($\mu g\,m^{-3}$)	AOD_{sat} (550 nm)	$\overline{\eta} = \frac{\overline{PM_{2.5,24\,h}}}{\overline{AOD_{sat}}}$ ($\mu g\,m^{-3}$)		$\frac{\overline{b_{ep,sat}}}{\overline{AOD_{sat}}}$ (Mm^{-1})	$\frac{\overline{b_{ep,sat}}}{\overline{b_{ep,24\,h}}}$	$\frac{\overline{b_{ep,24\,h}}}{\overline{PM_{2.5,24\,h}}}$ ($m^2\,g^{-1}$)	$\frac{\overline{PM_{2.5}}}{\overline{PM_t}}$	SO_4^{2-} ($\mu g\,m^{-3}$)	NO_3^{2-} ($\mu g\,m^{-3}$)
		Lat.	Long.	Empirical			GEOS-Chem[a]	Empirical					
Bandung, Indonesia	Jan–Apr 2014	−6.888	107.610	30.2 ± 0.3	0.26 ± 0.02[c]	116[c] ± 9	[32–54]	TBD	0.90 ± 0.04	20.8 ± 2.2	1.97	5.1	0.6
Dalhousie University, Canada	Jan–Oct 2013	44.638	−63.594	3.2 ± 0.2	0.09 ± 0.01	66 ± 4	[25–57]	257 ± 6	0.62 ± 0.02	12.3 ± 0.6	1.27	1.2	0.2
Emory University, USA	Jan–Mar 2014	33.688	−84.290	8.0 ± 0.3	0.09 ± 0.02	87 ± 19	[51–104]	601 ± 30	1.29 ± 0.03	5.5 ± 0.2	1.65	0.90	0.27
Ilorin University, Nigeria	Apr-May 2014	8.481	4.526	18.7 ± 1.1	0.68 ± 0.07	27 ± 3	[20–41]	165 ± 7	0.93 ± 0.03	TBD	0.86	TBD	TBD
Indian Institute of Technology Kanpur, India	Dec 2013–May 2014	26.519	80.232	101 ± 9	0.51 ± 0.04	139 ± 19	[61–103]	508 ± 29	0.87 ± 0.01	6.9 ± 0.1	1.61	TBD	TBD
Manila Observatory, Philippines	Jan–Feb 2014	14.635	121.077	TBD	0.22 ± 0.03	TBD	[35–57]	251 ± 50	0.63 ± 0.02	TBD	TBD	TBD	TBD
Mexico City	Jan–Dec 2013	19.333	−99.182	24.4 ± 0.4	0.27 ± 0.01	90 ± 4	[79–137]	n/a	n/a	n/a	n/a	n/a	n/a
NCU, Taiwan[b]	Jan–Dec 2012	24.968	121.185	22 ± 0.3	0.31 ± 0.02	71 ± 5	[31–73]	n/a	n/a	n/a	n/a	n/a	n/a
Tsinghua University, China	Feb–April 2013 and Nov 2013–Mar 2014	39.977	116.380	82.9 ± 8.1	0.56 ± 0.06	155 ± 6	[47–158]	565 ± 15	0.81 ± 0.01	4.9 ± 0.1	1.01	9.6	7.1
University of Dhaka, Bangladesh	Nov 2013–May 2014	23.728	90.398	32.6 ± 2.9	0.90 ± 0.07	69[c] ± 2	[49–73]	359 ± 4	0.63 ± 0.01	12.7 ± 0.5	0.79	4.5	0.7

Subscripts "sat" indicates periods averaged between 10:00 to 14:00 LT.
[a] Calculated GEOS-Chem η values (from 2001 to 2006) are from van Donkelaar et al. (2010), matched for the given empirical monthly-mean sampling periods.
[b] NCU data as reported from hourly BAM $PM_{2.5}$.
[c] AOD from previous year (for same seasonal time interval as $PM_{2.5}$ sampling).

Table A1. Comparison of hourly $PM_{2.5}$ measured at a site vs. predicting using Eq. (1) and a nephelometer at different sites. We define "satellite hours" as from 10:00 to 14:00 LT. For all sites a RH < 80 % cut-off was used to filter humid data.

Nephelometer site	Hourly $PM_{2.5}$ site	Distance between sites	# of obs	Year Span	Mean 24 h/midday $PM_{2.5}$	24 h error, $1\sigma_{24\,h}$ ($1\,\mu g\,m^{-3} + X$ %), R^2	Satellite error, σ_{sat} ($1\,\mu g\,m^{-3} + X$ %), R^2
MACA[a]	Oak[b]	14 km	3396	2008–2009	10.5 / 9.4	16.5 %, $R^2 = 0.87$	4.9 %, $R^2 = 0.96$
ROMA[a]	Fish[b]	33 km	1818	2007–2009	10.9 / 10.2	15.4 %, $R^2 = 0.51$	12.2 %, $R^2 = 0.66$
NACA[a]	Wash[b]	3.4 km	10302	2003–2009	10.3 / 9.3	16.6 %, $R^2 = 0.80$	10.2 %, $R^2 = 0.89$
Merged	–	–	**14 688**	–	**10.4 / 9.4**	**16.8 %, $R^2 = 0.79$**	**11.7 %, $R^2 = 0.85$**
Tsinghua U	US Emb	8 km		**2013**	**141 / 122**	**17.1 %, $R^2 = 0.88$**	**17.3 %, $R^2 = 0.94$**

[a] IMPROVE Sites (lat,long): MACA(37.037, −86.148), ROMA(32.791, −79.657), NACA(38.900, −77.040).
[b] EPA Sites (lat,long): Oak(37.037, −86.251), Fish(32.791, −79.959), Wash(38.922, −77.013).

Table A2. Site locations of SPARTAN monitors and the collocated reference instruments for pilot study.

City (University)	Latitude	Longitude	Reference light scatter	Reference $PM_{2.5}$ filter	Reference PM_{coarse} filter
Halifax (Dalhousie)	+44.638°	−63.594°	DustTrak[a], Dylos[b], Aurora[c]	Partisol[e], BAM[f]	Partisol[e]
Atlanta (Emory)	+33.798°	−84.323°	GRIMM[d]	PEM[g]	None
Beijing (Tsinghua)	+39.997°	+116.329°	DustTrak[a]	TEOM[h], BAM[f], Laoying[i]	None

[a] DustTrak model 8533 in Halifax, model 8530 in Beijing (TSI).
[b] Dylos DC1700 (Dylos).
[c] Aurora 3000 (Ecotech).
[d] GRIMM model 1.109 (GRIMM).
[e] Partisol 2025 (Thermo Scientific).
[f] Beta attenuation monitor 1020 (Met One).
[g] Personal environmental monitor model 761-203B (PEM).
[h] Tapered element oscillating microbalance series 1400a with a 50 °C sample stream (Thermo Scientific).
[i] Laoying model 2030 using 90 mm PTFE filters (Laoying).

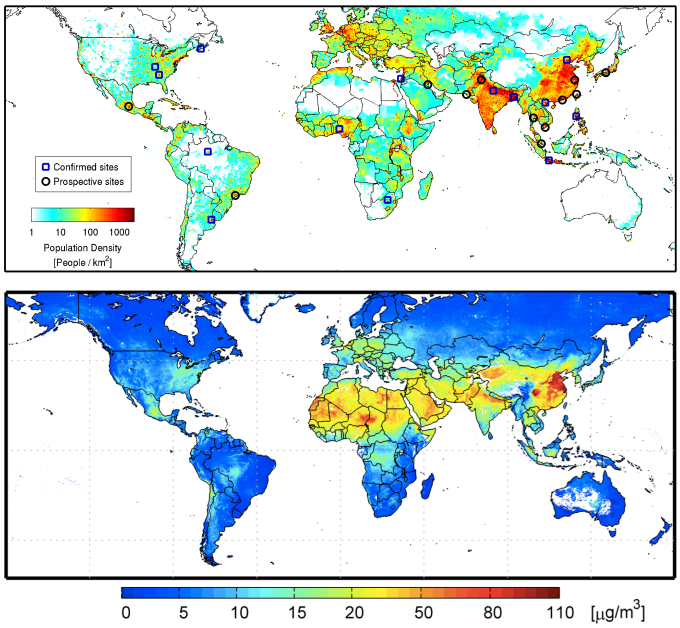

Figure 1. Top: global population density for 2010 (http://sedac.ciesin.columbia.edu). Black circles indicate priority sites for SPARTAN. Blue squares indicate confirmed sites. Table 1 contains further site information. Bottom: satellite-derived $PM_{2.5}$ ($\mu g\,m^{-3}$) averaged from 2001–2006 (at 10 km × 10 km resolution) as inferred from AOD from the MODIS and MISR satellite instruments and coincident GEOS-Chem CTM aerosol vertical profiles (van Donkelaar et al., 2010). White space indicates water or locations containing < 50 valid AOD retrievals during this period.

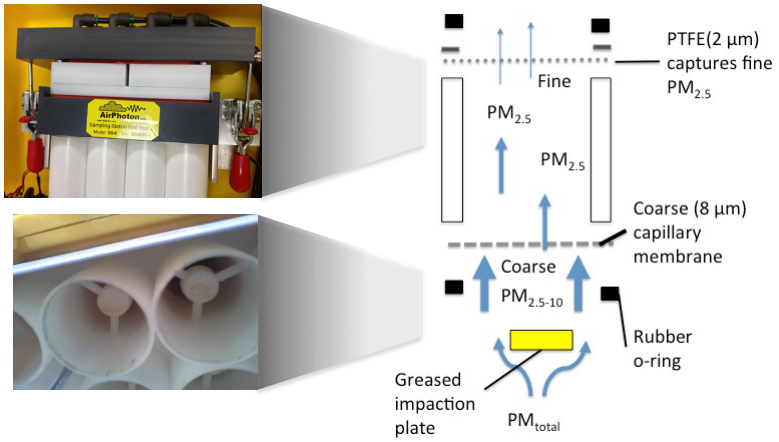

Figure 2. Diagram of AirPhoton filter assembly. The aerosol/air stream first passes through a bug screen followed by a greased impaction plate that removes particulates larger than ~ 10 µm diameter. Impaction plates are re-greased prior to loading a new cartridge. The 8 µm capillary membrane filter then traps coarse $PM_c \equiv (PM_{10} - PM_{2.5})$ particulates. A 2 µm PTFE filter traps fine $PM_{2.5}$. Blue arrows indicate the direction of airflow (flow rate = 4 L min^{-1}). Useable filter diameter on which PM is collected is 19 mm resulting in PTFE and capillary membrane face velocities of 23.5 cm s^{-1}. Capillary porosity is 5 %.

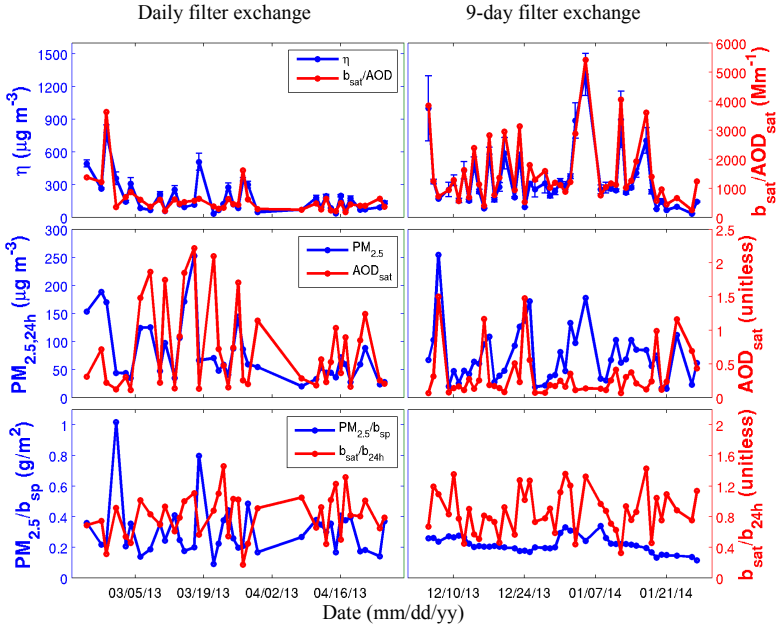

Figure 3. Temporal variation in Beijing, China of η (calculated as the mean 24 h $PM_{2.5}$ divided by mean AOD at satellite overpass times) and related variables. Error bars represent 1σ measurement uncertainty ($\sigma_{PM_{2.5}}$ = 1 µg m^{-3}, σ_{AOD} = 0.02). The left column (February–April 2013) used daily sampled filters while the right column (December 2013–January 2014) sampled each filter intermittently over 9 days.

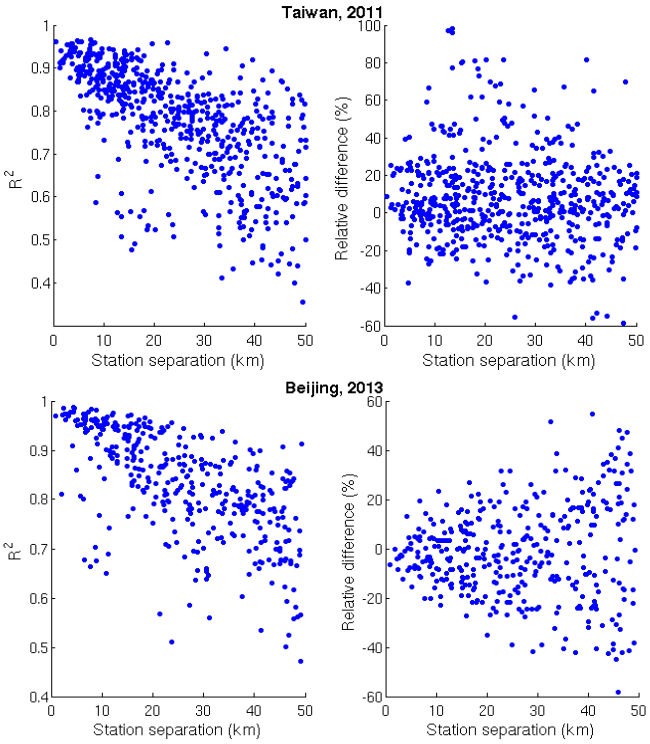

Figure A1. $PM_{2.5}$ relationships between pairs of stations in Taiwan (2011 calendar year) and Beijing (2013 calendar year). There were 76 stations available in Taiwan for comparison and 36 available in Beijing.

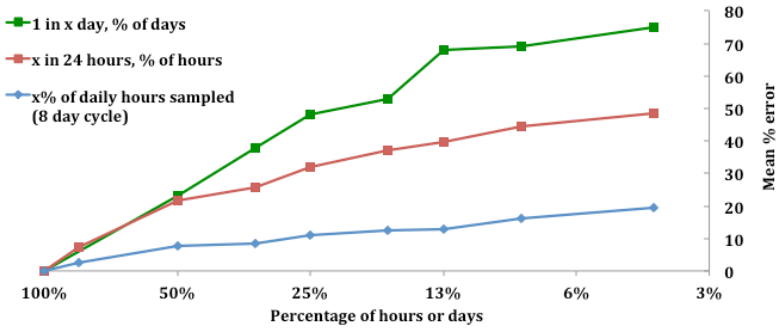

Figure A2. Relative errors representing annual mean $PM_{2.5}$ obtained from 100 EPA sites averaged over various hourly periods for 2006. Sampling periods are divided into **(a)** 1-in-x (x = 1 to 24) day sampling intervals (green squares), **(b)** fraction of day (1 to 24 h day^{-1}, red squares), and **(c)** staggering x % of hours per day during an 8 day cycle (blue diamonds).

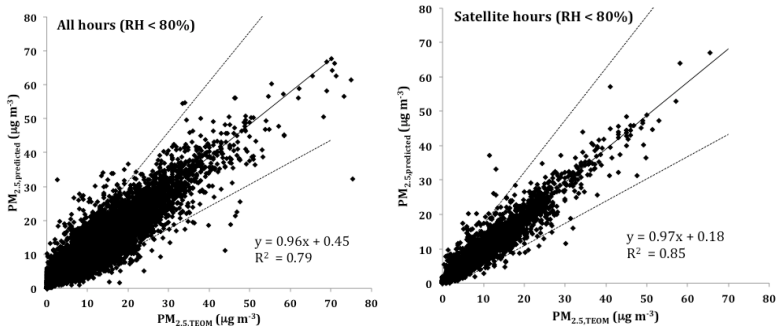

Figure A3. Comparison of predicted hourly fine mass vs. measured TEOM $PM_{2.5}$ for combined NACA, ROMA, and MACA sites (for RH < 80 %). Dashed lines show 2 σ confidence interval for predicted $PM_{2.5}$ RMA slope.

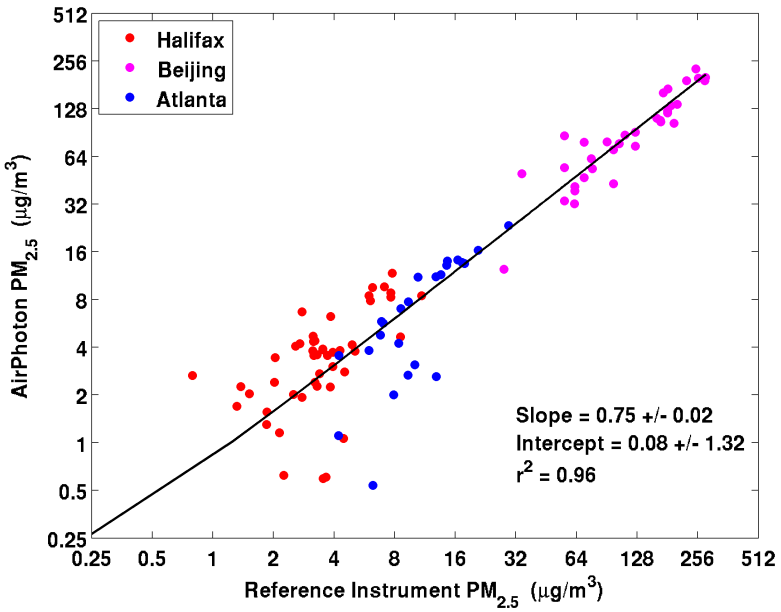

Figure A4. Scatter plot shows reduced major axis (RMA) regression for Beijing, Atlanta and Halifax $PM_{2.5}$ concentrations, respectively. AirPhoton filter samplers in Halifax, Atlanta and Beijing were referenced using Partisol, PEM and Laoying air sampler instruments, respectively.

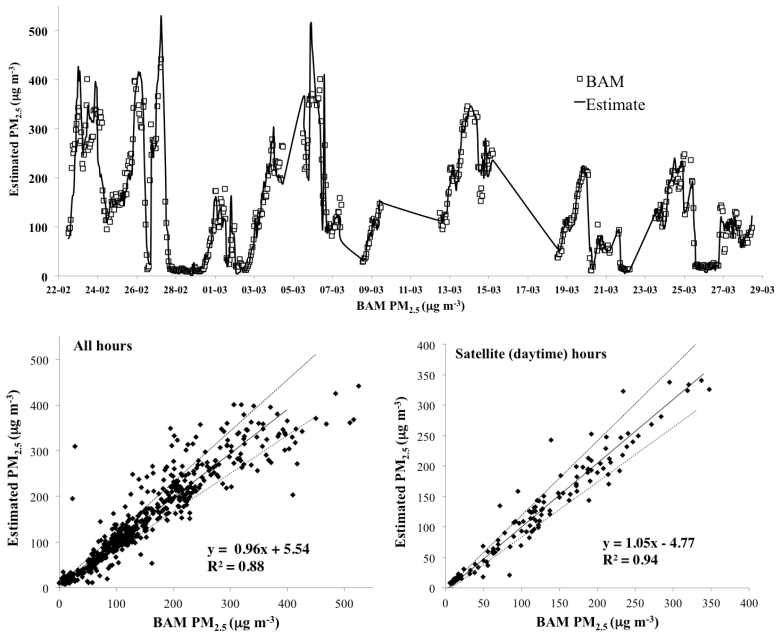

Figure A5. Top: evaluation of hourly $PM_{2.5}$ in Beijing from 24 February to 29 March 2013, reconstructed from the AirPhoton nephelometer and compared to a $PM_{2.5}$ reference instrument (BAM) located 8 km away. Bottom: hourly comparison between all-day and satellite $PM_{2.5}$ estimates. The percent difference with respect to RMA line is $1\,\mu g\,m^{-3} + 17\,\%$ for both all hours and satellite overpass hours. Dashed lines display the $1\,\sigma$ confidence boundary.